Journal of Applied Mechanics and Technical Physics, Vol. 42, No. 1, pp. 57–62, 2001

DEVELOPMENT OF NATURAL DISTURBANCES IN A HYPERSONIC BOUNDARY LAYER ON A SHARP CONE

D. A. Bountin, A. A. Sidorenko, and A. N. Shiplyuk

UDC 532.526

Experimental data on the location of the laminar–turbulent transition and development of natural disturbances in a laminar hypersonic boundary layer on a sharp thermally insulated cone with a half-angle of 7° are presented. The existence of the second mode of disturbances is confirmed. It is shown that the transition is determined by the first mode of disturbances. The experimental data are in good agreement with theoretical calculations.

Development of space technology and aviation requires the study of the processes that occur in a hypersonic boundary layer and cause the laminar–turbulent transition. The mechanisms of transition at hypersonic velocities have been poorly studied. This is related to the fact that experiments and theoretical analysis are very complicated. The physical processes of the laminar–turbulent transition at hypersonic velocities are qualitatively different from those typical of subsonic and supersonic flows. The main reason for this difference is the appearance of instability modes of the acoustic type (second, third modes, etc.), which were theoretically predicted by Mack. According to the calculations of [1], the second mode of disturbances plays the dominating role in the laminar–turbulent transition beginning from the Mach number $M \approx 4$.

The second mode was first found by Kendall in 1967 in experiments on a flat plate. He showed [2] using a cone model that this type of instability plays the determining role in the laminar–turbulent transition for $M = 8.5$. At the same time, for $M = 4.5$ and 5.6, the expected domination of the second mode was not observed. The data obtained for these Mach numbers were in qualitative agreement with Mack's calculations [1]. The experiments of [3] confirmed the existence of the second mode of disturbances and gave additional data on the stability of a hypersonic boundary layer. In particular, Mack's conclusion about the destabilization of the second mode upon cooling the model surface was confirmed. The studies of [4] on a cylinder and cones with half-angles of 7° for $M = 8$ may be mentioned as the most complete data. These experiments yielded the amplitude amplification rates for disturbances with frequencies corresponding to the first and second modes and the curves of neutral stability. In addition, the effect of nose bluntness and the angle of attack on the model on the boundary-layer stability was studied on cones. The dominating role of the second mode in the laminar–turbulent transition on a sharp cone was demonstrated. In the experiments with a hollow cylinder [5], the expected domination of the second mode was not observed. The calculations of Malik [6] show that first-mode disturbances may exert a decisive effect on the laminar–turbulent transition for the case of an adiabatic wall on a sharp cone up to $M \approx 7$. The second-mode disturbances were not observed by Wendt and Simen [7] on a flat plate for $M = 5$, which is possibly related to the limited frequency range of the transducer used. The stability of the boundary layer with an adverse pressure gradient (the pressure increased downstream) on a cone for $M = 5.91$ was studied in NASA on an M6NTC quiet wind tunnel [8]. The data obtained confirm the main conclusions of Mack's calculations. It is argued [8] that the transition is caused by the second mode, but this cannot be concluded unambiguously on the basis of the data given in that paper.

Institute of Theoretical and Applied Mechanics, Siberian Division, Russian Academy of Sciences, Novosibirsk 630090. Translated from Prikladnaya Mekhanika i Tekhnicheskaya Fizika, Vol. 42, No. 1, pp. 65–71, January–February, 2001. Original article submitted March 27, 2000.

0021-8944/01/4201-00057 $25.00

The objective of the present work is to obtain additional experimental data on stability of a hypersonic boundary layer: to determine the transition Reynolds numbers, the mean and fluctuating characteristics of the boundary layer, and the amplification rate of disturbances.

1. Experimental Equipment. The experiments were conducted in the T-326 hypersonic blowdown wind tunnel of the Institute of Theoretical and Applied Mechanics of the Siberian Division of the Russian Academy of Sciences for a free-stream Mach number $M_\infty = 5.92$, unit Reynolds number $Re_{1\infty} = 12.5 \cdot 10^6$ m^{-1}, stagnation pressure $P_0 = 9.8 \cdot 10^5$ Pa, and stagnation temperature $T_0 = 380$ K. The values of the stagnation parameters P_0 and T_0 were maintained constant during the experiment within 0.9% for temperature and within 0.1% for pressure. The free-stream characteristics M_∞ and $Re_{1\infty}$ were determined from the measured P_0 and T_0 and the known dependence $M_\infty = f(P_0)$ obtained by studying the flow field in the test section of the T-326 wind tunnel. The oscillations were measured by a constant-temperature hot-wire anemometer, which had a frequency range from 0 to 500 kHz. Single-wire probes were used; they were manufactured from a tungsten wire 5 μm in diameter and 1.3 mm long. The wire overheating was $\tau = (T_w - T_e)/T_0 = 0.4$ (T_w is the wire temperature and T_e is the gas-recovery temperature on the wire); therefore, it was assumed during data processing that the hot-wire anemometer is sensitive only to mass-flow oscillations, and the receptivity coefficient was assumed to be equal to 0.25 [9].

During the measurement of transverse distributions in the boundary layer, the hot-wire probe moved away from the model wall with a step of 0.05 mm. The error of coordinate determination was 0.01 mm. The zero position of the probe at the model surface was verified using the electric contact.

In the course of the experiment, the variable and constant components of the electric signal from the hot-wire anemometer output were recorded into the computer memory by means of two 12-bit analog-to-digital converters. To obtain oscillation spectra, the variable signal was digitized with a frequency of 1.25 MHz, which allowed us to perform a spectral analysis up to a frequency of 612 kHz.

The model was a sharp steel cone 0.5 m long with a half-angle of 7°. The bluntness radius of the model nose tip was less than 0.1 mm. For model mounting at zero angles of attack and sideslip, four orifices were made over the model radius at an identical distance from each other. The zero angle was determined from the condition of equal static pressure in all orifices. The error of the angle of model inclination was 0.1°. Since the model was rather large, it did not have enough time to warm up in the beginning of the experiment; therefore, an electric heater was placed inside the model to satisfy the condition of adiabaticity. The wall temperature $T_w \approx 320$ K was controlled by a thermocouple built into the model and located near the model surface.

2. Location of the Laminar–Turbulent Transition. The data on the laminar–turbulent transition were obtained by a Pitot probe whose thickness was 0.7 mm. A strain-gage transducer with the range of 0–10^5 Pa was used for pressure measurements. The measurement error was 0.5%.

During the experiment, the probe moved inside the boundary layer over the cone surface along its generatrix. The error of coordinate determination was 0.1 mm.

The maximum in the Pitot pressure distribution P_0' along the x coordinate corresponded to the end of the laminar–turbulent transition. The measurements were performed within the range $Re_{1\infty} = (12.2\text{–}22.6) \times 10^6$ m^{-1} [$P_0 = (9.8\text{–}19.5) \cdot 10^5$ Pa].

Figure 1 shows the transition Reynolds number Re_{tr} based on the parameters at the boundary-layer edge versus the Mach number at the boundary-layer edge. Figure 1 was borrowed from [6], and the data obtained in the present study were added.

It is seen that the transition Reynolds numbers obtained in the T-326 wind tunnel (which is not a quiet facility) are much higher than curve 3. Possible reasons are discussed below.

3. Spectra of Disturbances in the Boundary Layer. The distributions of disturbance spectra in the boundary layer were measured in 17 cross sections. For six of them, Fig. 2 shows the distributions of the root-mean-square amplitudes of integral fluctuations of the mass flow $\langle \rho u \rangle$ normalized to the mean mass-flow rate (Fig. 2a) and the mean velocities U (Fig. 2b). The ordinate axis is the y coordinate normalized

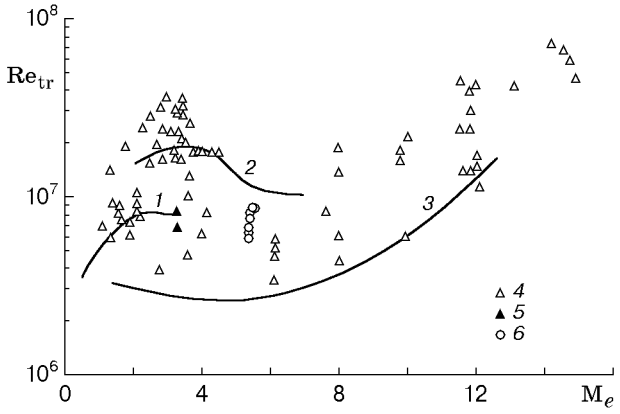

Fig. 1. Transition Reynolds number versus the Mach number at the boundary-layer edge: curves 1 and 2 refer to calculations by the method of e^n ($n = 10$) for the adiabatic and cooled walls, respectively, and curve 3 refers to the experimental data for conventional wind tunnels; the points refer to the results of flight tests (4), experimental data for quiet wind tunnels (5), and results of the present tests in T-326 for $\mathrm{Re}_{1\infty} = (12.2\text{–}22.6) \cdot 10^6$ m^{-1} (6).

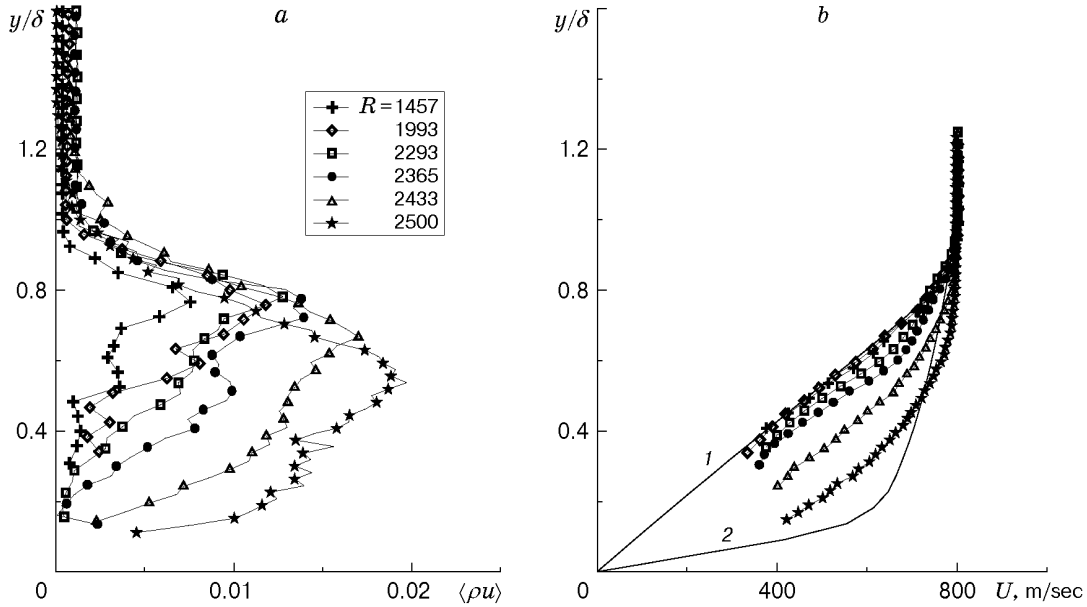

Fig. 2. Distribution of the root-mean-square integral oscillations (a) and mean velocity (b) across the boundary layer.

to the boundary-layer thickness δ. The y coordinate was counted from the model surface perpendicular to its axis; R is the root of the Reynolds number: $R = \sqrt{\mathrm{Re}_{1e}x}$ (Re_{1e} is the unit Reynolds number based on the parameters at the boundary-layer edge and x is the coordinate along the cone generatrix). The parameters at the boundary-layer edge were found by inviscid conical flow calculations. The boundary-layer thickness was determined from the mean-velocity distribution under the condition $U = 0.99U_e$, where U_e is the stream velocity near the boundary-layer edge. Curve 1 in Fig. 2b corresponds to the velocity profile for a laminar boundary layer calculated on the basis of boundary-layer equations; curve 2 is the calculation of the velocity profile for a turbulent boundary layer by the formula $U/U_e = (y/\delta)^{1/7}$ taking into account the existence of a laminar sublayer; the points are experimental data. It is seen from Fig. 2b that the boundary layer remains laminar for $R < 2300$: the measured velocity profiles coincide with the calculated laminar profile (curve 1), and the oscillations are small and concentrated in a rather narrow region in the vicinity of $y \approx 0.8\delta$. For $R > 2300$, the profiles of the mean velocities and amplitudes of integral oscillations become more full, and the level of oscillations increases almost twice as compared to the laminar region, which indicates the beginning of boundary-layer turbulization. In addition, a dramatic increase in the boundary-layer thickness was observed.

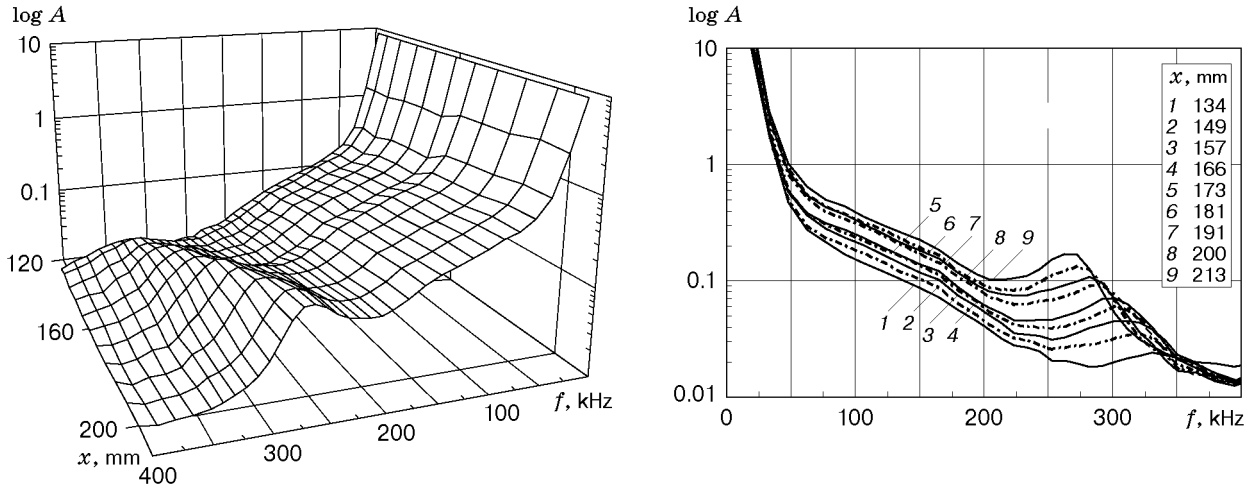

Fig. 3. Distribution of the spectrum of natural disturbances in the layer of the maximum oscillations.

To determine the amplification rates of instability waves, we performed the measurements in the layer of the maximum disturbances using the standard technique (see, e.g., [10]). It follows from the experimental data obtained that the relative vertical coordinate y/δ of the position of the layer of the maximum disturbances and the mean voltage at the hot-wire probe located in this layer are constant for a hypersonic laminar boundary layer. Therefore, further experiments were performed as follows. First, the position of the layer of the maximum disturbances and the mean voltage in this layer were determined. Then, the probe moved along the cone generatrix to keep the voltage constant. The oscillation spectrum was recorded with a step of approximately 2 mm along the x coordinate. The position of the maximum of disturbances was checked several times in the course of the experiment, and the position of the probe was corrected if necessary. These measurements were not performed in the regions of transition and developed turbulence.

The distributions of the spectra of natural disturbances in the layer of the maximum oscillations are plotted in Fig. 3 (A is the Fourier amplitude of mass-flow fluctuations). It is seen from Fig. 3 that the disturbances of all frequencies increase. We note that a peak of disturbances is observed at frequencies of 250–350 kHz. The estimate of the wavelength λ of these disturbances with the use of the phase velocity calculated by the locally parallel linear theory of stability shows that λ is approximately equal to two boundary-layer thicknesses (the phase velocity is $C_x = 0.92$; the method of C_x calculation is similar to the technique used in [11]). This value of λ corresponds to the theoretical [1] and experimental values of the wavelength of the second mode of disturbances [12]. The dimensionless frequency $F = 2\pi f/(\mathrm{Re}_{1e}U_e) = (1.0\text{–}1.5) \cdot 10^{-4}$ is also in agreement with the second-mode frequency. Hence, the peak at high frequencies corresponds to the second mode of disturbances. We can trace the evolution of this peak: an increase in amplitude and a shift of the maximum of disturbances toward lower frequencies. This behavior is typical of the second-mode disturbances. As was noted above, the wavelength of this mode is approximately 2δ; therefore, the wavelength increases downstream with increasing δ, and the frequency decreases.

4. Amplification Rates of Disturbances. To calculate the amplification rates of disturbance waves, the amplitude distributions of oscillations in terms of R measured in the maximum of disturbances (Fig. 3) were smoothed and approximated by a polynomial. The amplification rates were calculated using the formula $-\alpha_i = 1/(2A)(\partial A/\partial R)$.

The results of data processing are shown in Figs. 4–6. Figure 4 shows that the amplification rates of low-frequency disturbances corresponding to the first mode remain almost unchanged and are greater than zero within the entire range of measurements. The amplification rates of high-frequency disturbances have a clear maximum and become negative with increasing R. A peak in the frequency range corresponding to the second mode of disturbances is clearly seen in Figs. 5 and 6. Though the main energy belongs to low-frequency oscillations, the second-mode waves were most unstable, which corresponds to theoretical pre-

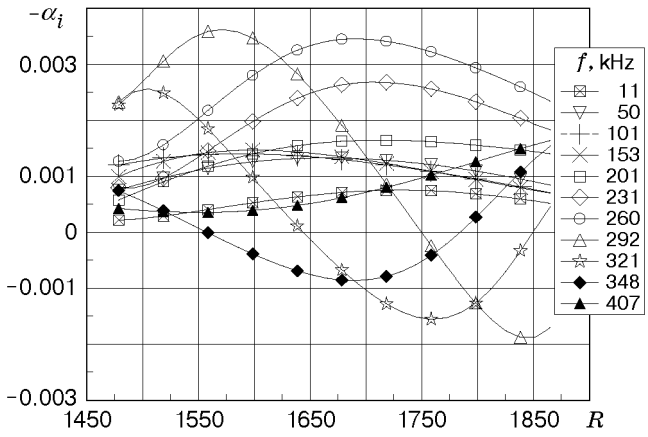

Fig. 4

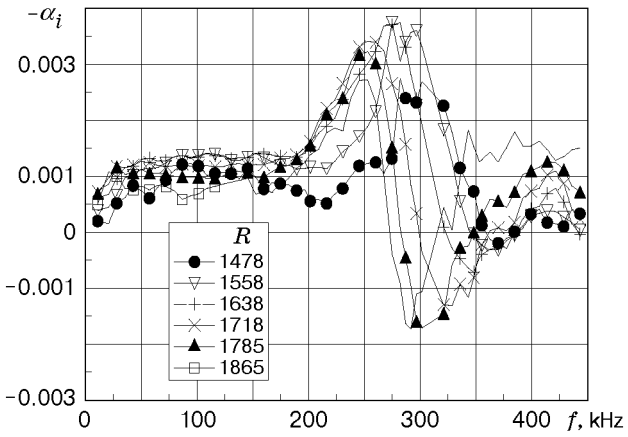

Fig. 5

Fig. 4. Distributions of the amplification rates of disturbance waves for different frequencies.

Fig. 5. Distributions of the amplification rates of disturbance waves for different values of R.

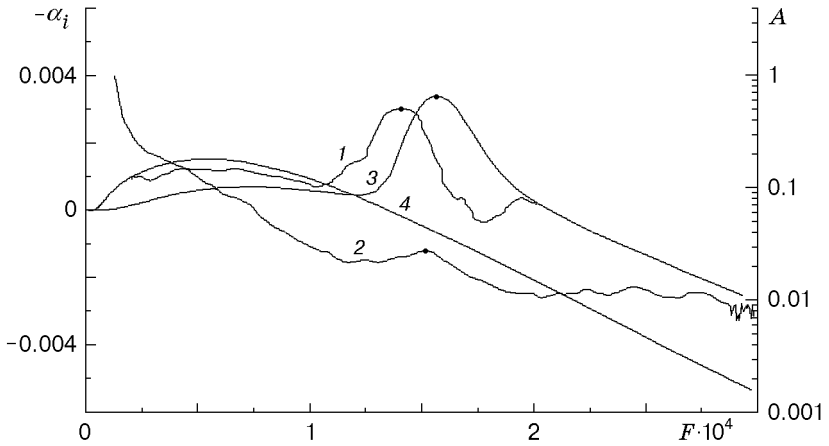

Fig. 6. Dependences of the amplification rates (curves 1, 3, and 4) and wave amplitude (curve 2) on the dimensionless frequency for $R = 1600$: curves 1 and 2 refer to experiments and curves 3 and 4 refer to calculations [$\theta = 0$ (3) and 50° (4)]; the points are local maxima corresponding to the second mode.

dictions. A decrease in frequency is observed in Fig. 5 with increasing R for oscillations with the maximum amplitude amplification rates, which is also in agreement with theoretical results. It is seen in Fig. 6 that the numerical and experimental data on $-\alpha_i$ are in good qualitative and quantitative agreement. The calculation was performed on the basis of the locally parallel linear theory of stability. The disagreement of the experimental and theoretical frequencies corresponding to the amplitudes of waves with the maximum amplification rates can be also noted in Fig. 6. The reason may be the neglect of the effect of flow nonparallelism on the boundary-layer stability in calculations.

The difference in experimental and theoretical values of $-\alpha_i$, which was also observed in [12], may be caused by an incorrect comparison of these data. The numerical data were obtained for a wave with a certain angle of inclination θ, whereas the values of α_i based on experimental data were determined on the basis of integral-amplitude distributions, since it is impossible to identify waves with a certain angle of inclination in the course of measurement of the characteristics of natural disturbances. For a correct comparison, it is necessary to use experiments with the technique of artificial disturbances or correlation measurements.

It follows from the data obtained (see Fig. 3) that the main energy of free-stream oscillations is concentrated on low frequencies. Therefore, the initial amplitudes of the first-mode disturbances in the boundary layer are much higher than the second-mode amplitudes. Though the second-mode disturbances

increase faster (see Figs. 4–6), because of the low initial amplitudes of these disturbances, the main role in the laminar–turbulent transition belongs to slowly growing first-mode disturbances; this is a possible reason for the downstream shift of the transition region. This indicates that the effect of the first- and second-mode disturbances on the laminar–turbulent transition cannot be estimated without taking into account the level and spectrum of the initial disturbances of the boundary layer. Therefore, it is necessary to study the boundary-layer receptivity to free-stream perturbations, since the level and spectrum of boundary-layer oscillations depend on the free-stream disturbances.

Conclusions. Thus, the existence of the second mode is experimentally verified in the present paper. The amplification rates of the wave amplitudes for the first and second modes of instability are determined. It is shown that the second-mode disturbances have greater amplification rates, but despite this fact, the transition is determined by the first mode. Good agreement of the experimental data and calculations by the locally parallel linear theory of stability is obtained.

This work was supported by the Russian Foundation for Fundamental Research (Grant No. 98-01-00735) and International Science and Technology Center (Grant No. 128).

REFERENCES

1. L. M. Mack, "Boundary layer stability theory," Document No. 900-277, Rev. A, Jet Propulsion Laboratory, Pasadena (1969).
2. J. M. Kendall, "Wind tunnel experiments relating to supersonic and hypersonic boundary layer transition," *AIAA J.*, **13**, 290–299 (1975).
3. A. Demetriades, "Boundary layer instability observations at Mach number 7," *Trans. ASME, Ser. E, J. Appl. Mech.*, **44**, No. 1, 7–10 (1977).
4. K. Stetson and R. Kimmel, "On hypersonic boundary-layer stability," AIAA Paper No. 92-0737 (1991).
5. K. Stetson, E. Thompson, J. Donaldson, and L. Siler, "A comparison of planar and conical boundary layer stability and transition at Mach number 8," AIAA Paper No. 91-1639 (1991).
6. M. R. Malik, "Prediction and control of transition in supersonic and hypersonic boundary layers," *AIAA J.*, **27**, No. 11, 1487–1493 (1995).
7. V. Wendt and M. Simen, "An experimental and theoretical investigation of instabilities in hypersonic flat plate boundary layer flow," *Phys. Fluids*, No. 7, 877–887 (1995).
8. S. Wilkinson, "A review of hypersonic boundary layer stability experiments in a quiet Mach 6 wind tunnel," AIAA Paper No. 97-1819 (1997).
9. D. Bestion, J. Gaviglio, and J. P. Bonnet, "Comparison between constant-current and constant-temperature hot-wire anemometers in high-speed flows," *Rev. Sci. Instrum.*, **54**, No. 11, 1513–1524 (1983).
10. V. A. Lebiga, A. A. Maslov, and V. G. Pridanov, "Experimental investigation of the stability of supersonic boundary layer on a flat insulated plate," *Arch. Mech.*, **31**, No. 3, 397–405 (1979).
11. S. A. Gaponov and A. A. Maslov, "Stability of a compressible boundary layer at subsonic velocities," *Izv. Sib. Otd. Akad. Nauk SSSR, Ser. Tekh. Nauk*, Issue 1, No. 3, 24–27 (1971).
12. K. F. Stetson, E. R. Thompson, J. C. Donaldson, and L. G. Siler, "Laminar boundary layer stability experiments on a cone at Mach 8. Part 1. Sharp cone," AIAA Paper No. 83-1761 (1983).